Real-time Coupling Coefficient Estimation and Maximum Efficiency Control on Dynamic Wireless Power Transfer Using Secondary DC-DC Converter

Daita Kobayashi*, Takehiro Imura**, Yoichi Hori***
The University of Tokyo
5-1-5, Kashiwanoha, Kashiwa, Chiba, 277-8561, Japan
Phone: +81-4-7136-3881
Email: kobayashi14@hflab.k.u-tokyo.ac.jp*, imura@hori.k.u-tokyo.ac.jp**, hori@k.u-tokyo.ac.jp***

***Abstract*—Transmitting efficiency is able to be controlled by changing the input impedance on the receiving side using a DC-DC converter for static wireless power transfer system. However, the control method has never been applied for dynamic wireless power transfer system where coupling coefficient changes drastically. The information of coupling coefficient is needed constantly to achieve the control. Moreover, the considerations about dynamics of the transmitting circuit and coupling coefficient are necessary in dynamic wireless power transfer system. In this paper, a simple method of coupling coefficient estimation with RLS (Recursive least squares) filter and maximum efficiency control using a PID feedback controller are proposed. The simulation and experimental results of dynamic maximum efficiency control are provided and indicating the effectiveness of the proposed control in a real dynamic wireless power transfer system for EVs.**

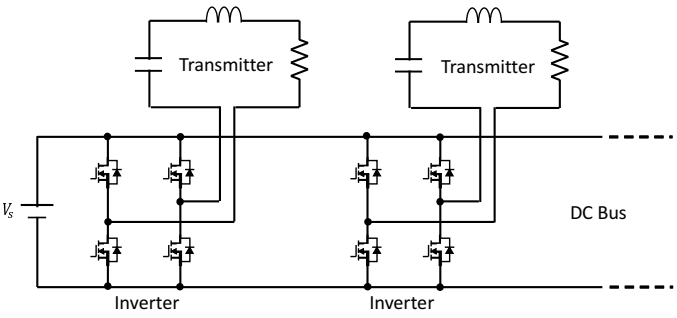

Fig. 1. Proposed transmitting side (DC bus system).

I. Introduction

Wireless power transfer (WPT) via magnetic resonant coupling was invented in 2007 by MIT [1]. That gave an enormous impact to the world and the technology is being researched all over the world nowadays. WPT technology has huge potential to be applied to many kinds of fields such as transportation, home appliances [2], medical appliances [3] and so on. Especially among them, the application to electric vehicles (EVs) is one of the hottest topics in WPT society [4], [5]. That is because WPT is able to solve the problems that EVs potentially has such as its short cruising range, long charging process. Therefore, static wireless power transfer for EVs (wireless charging when EVs are not in motion) has been researched from many kinds of point of view: coil structure [6], circuit configuration [7], the control method of power converter [8]. Furthermore, dynamic wireless power transfer (DWPT) (wireless charging while EVs are in motion) has been attracting more attention in recent years. With DWPT, EVs would be able to obtain longer cruising distance because they can travel while receiving power from infrastructure. Moreover, they do not need to carry a large amount of heavy and bulky batteries, which leads to the reduction of the EVs' cost.

In order to propagate DWPT as a substitute for normal charging, it has to be simple and easy to install. On the other hand, the secondary side can be complex and should optimize power transmitting characteristic. For instance, transmitting efficiency can be optimized by adjusting the secondary voltage to optimal voltage with power converters such as DC-DC converters [9], [10]. However, these control methods use the information of the coupling coefficient which changes constantly and is not directly measurable. In the paper [11], a method to estimate coupling coefficient and real-time maximum efficiency control were introduced. Yet, the secondary voltage which has maximum efficiency was not tracked well enough because the control of DC-DC converter was just based on static feed forward control.

In this paper, an structure of DWPT system optimized for the transmitting efficiency is introduced. Moreover, a simple method of coupling coefficient estimation and a control method of a DC-DC converter based on dynamic feedback control which has better characteristics of tracking the maximum efficiency point than the previous research are proposed.

In section II, the proposed DWPT system structure is introduced. In section III, the basic ideas to track maximum efficiency and to estimate coupling coefficient between a transmitter and a receiver are explained. Furthermore, the modeling and the control method of a DC-DC converter for DWPT system are introduced in section IV. Lastly, the simulation results and the experimental results using experimental setup which simulates DWPT for EVs are provided in section V.

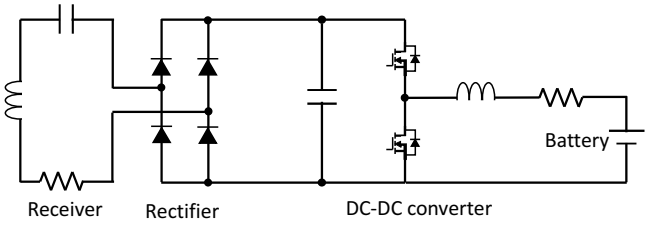

Fig. 2. Proposed receiving side.

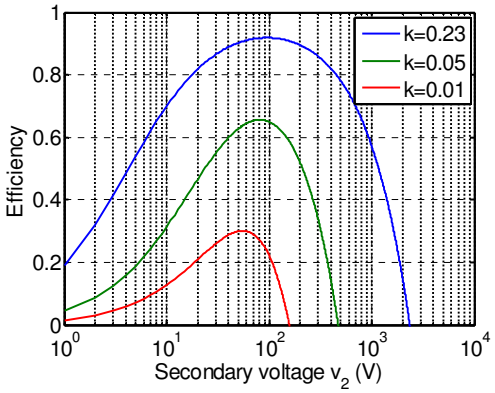

Fig. 3. Transmitting efficiency at different V_2 (V_1=100 V).

II. Proposed System Structure for DWPT

A. Transmitting side

Many research institutes have proposed the structure of the coils on primary side (road side) for DWPT [12], [13]. Most structures can be categorized in two groups: "Single-coil design" and "segmented coil design" [14]. Although both structures have their advantages, "segmented coil design" is chosen as a target of this research because of its high efficiency and limited magnetic field leakage.

Fig. 1 shows the considered design of the transmitting side of DWPT which is called "DC bus system". A transmitter consists of just one series-compensated transmitting coil and an inverter. A DC bus is laid below and each transmitter is connected to it in parallel. This simple structure makes maintenance and placement easy. In addition, high power transfer is possible because each inverter bears power for just one transmitter coil. Furthermore, the DC bus reduces EMI compared to a long AC bus.

B. Receiving side

Since the transmitting side is simple enough, the receiving side should have some degree of freedom in control. Fig. 2 illustrates the considered structure of receiving side. The receiving side is composed of a series-compensated receiving coil, a rectifier, a DC-DC converter and a storage such as battery or super capacitor. The DC-DC converter changes the secondary voltage V_2 in order to control the transmitting efficiency.

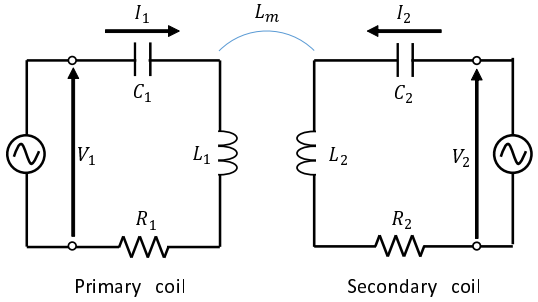

Fig. 4. Model of WPT with the simplified secondary side.

III. Maximum Efficiency Control and Real-Time Coupling Coefficient Estimation

A. Maximum efficiency control

For simplicity, the WPT model that has a constant voltage source and a constant voltage load is targeted. Fig.3 shows the change in the transmitting efficiency at different secondary voltages V_2 (RMS value). Fig. 3 shows that the efficiency depends on V_2 and has a peak at a certain voltage ($V_{2\eta max}$), which is derived as (1) [10].

$$V_{2\eta max} = \sqrt{\frac{R_2}{R_1}} \frac{\omega_0 k \sqrt{L_1 L_2}}{\sqrt{R_1 R_2 + (\omega_0 k)^2 L_1 L_2} + \sqrt{R_1 R_2}} V_1 \quad (1)$$

Where R_1 , R_2 and L_1, L_2 are the resistances and the inductances of the primary and the secondary coils, respectively. k is coupling coefficient and ω_0 is resonant angular frequency. Thus, the important idea is that a WPT system is able to achieve maximum efficiency by adjusting V_2 to $V_{2\eta max}$.

B. Real-time coupling coefficient estimation

If WPT was carried out while a vehicle is in motion, the coupling coefficient k would constantly fluctuate although k is necessary to obtain $V_{2\eta max}$ (1). One of the solution to obtain the information of k is wireless information communication between the primary and secondary side. Yet, the interference between transferring power and the communication might become another problem. Therefore, k should be estimated from the secondary voltage and current [15]. It is known that magnetic induced secondary current has a phase delay of 90 degrees to the primary current. The secondary side in Fig. 2 has squared secondary voltage whose amplitude is the same voltage as the DC-link capacitor. Moreover, the secondary voltage has 180 degrees of phase difference between the secondary current in Fig. 4. Summarizing the above discussion and considering just fundamental waves of the primary and secondary voltages, we can model the secondary side as a ideal voltage source (Fig. 4).

From Fig. 4, Kirchhoff's Voltage Law (KVL) equation (2) is derived.

$$\begin{bmatrix} V_1 \\ jV_2 \end{bmatrix} = \begin{bmatrix} R_1 & j\omega_0 k\sqrt{L_1 L_2} \\ j\omega_0 k\sqrt{L_1 L_2} & R_2 \end{bmatrix} \begin{bmatrix} I_1 \\ -jI_2 \end{bmatrix} \quad (2)$$

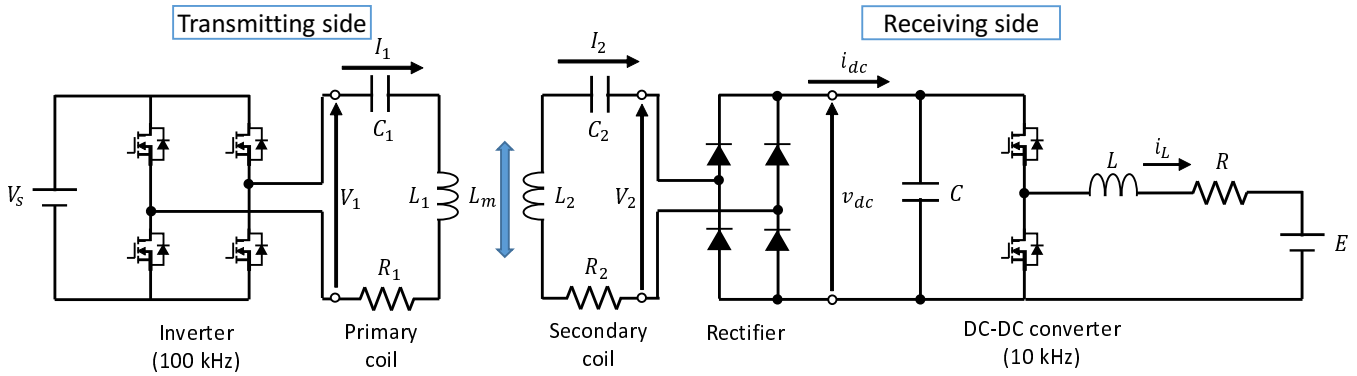

Fig. 5. Whole topology of the proposed DWPT system.

Thus, the coupling coefficient can be calculated as (3).

$$\hat{k} = \frac{V_1 \pm \sqrt{V_1^2 - 4R_1 I_2 \left(V_2 + R_2 I_2\right)}}{2I_2 \omega_0 \sqrt{L_1 L_2}} \tag{3}$$

Here, (3) has two solutions. The solution with a positive sign matches with its actual value only when k is large. On the other hand, the other solution matches the actual value only when k is small. In this study, the solution with a negative sign is neglected since we are just interested in the case that a receiver is close to a transmitter.

One of the large issues with the estimation method is sensor noise. In the proposed control method, estimated k is directly used to make the duty ratio command of DC-DC converter. Thus, recursive least square (RLS) filter is applied to reduce the sensor noise. From (3), output $y[i]$ and regressor $\phi[i]$ are determined as follows (i is a sampling point of a sensor.)

$$y[i] = V_1 + \sqrt{V_1^2 - 4R_1 I_2 \left(V_2[i] + R_2 I_2[i]\right)} \tag{4}$$

$$\phi[i] = 2I_2[i]\omega_0 \sqrt{L_1 L_2} \tag{5}$$

Here, RLS is used to estimate $\hat{k}$ statistically by updating $\hat{k}[i]$, $y[i]$ and $\phi[i]$ with following equations.

$$\begin{aligned} \hat{k}[i] &= \hat{k}[i-1] + \frac{\phi[i]P[i-1]}{\lambda + \phi[i]^2 P[i-1]}\epsilon[i] \\ \epsilon[i] &= y[i] - \phi[i]\hat{k}[i-1] \\ P[i] &= \frac{1}{\lambda}\left\{P[i-1] - \frac{\phi[i]^2 P[i-1]^2}{\lambda + \phi[i]^2 P[i-1]}\right\} \end{aligned} \tag{6}$$

Where, λ is forgetting factor, $\hat{k}[0] = 0$. $P[0] = 1$.
Another issue of the proposed k estimation method is that the KVL equation (2) does not have information of transient response of a WPT circuit. However, according to the study in [11], the real parts of the dominant poles in the transfer functions from the primary and secondary voltages to the secondary current are almost 10 times as fast as the fluctuation frequency of k even if a vehicle runs at 100 km/h over a 3 m long transmitter. In other words, coupling coefficient k is almost static from a viewpoint of general WPT circuit. Therefore, the KVL equation (2) is available for a EVs' DWPT system.

C. AC-DC transformation

Fig. 5 shows the whole picture of the proposed DWPT system. V_s is the voltage of DC voltage source, V_1 , V_2 and I_1 , I_2 are RMS value of the fundamental harmonics of the primary and the secondary voltage and current. v_{dc} is the voltage of the DC-link capacitor and i_{dc} is the mean value of the current which flows into the capacitor. i_L is the current which flows into the battery E. C is the capacitance of the DC-link capacitor, L is the inductance, R is the resistance of the smoothing choke coil. The secondary voltage that gives maximum transmitting efficiency (1) and coupling coefficient estimation equation (3) were introduced with RMS value in the previous section. However, current and voltage sensors with high band width are necessary to acquire RMS value of waves with hundreds of kHz. Therefore, the proposed control method uses only the DC values such as V_s, v_{dc}, i_{dc} in Fig. 5 to reduce the installation cost. In the DWPT system, the secondary current is a sinusoidal wave at the resonant frequency, and the secondary voltage is a square wave, which has the same amplitude as v_{dc} . Thus, when the primary inverter is operated with a square wave, V_1, V_2 and I_2 are expressed as follows using Fourier series expansions,

$$V_1 = \frac{2\sqrt{2}}{\pi}V_s, \quad V_2 = \frac{2\sqrt{2}}{\pi}v_{dc}, \quad I_2 = \frac{\pi}{2\sqrt{2}}i_{dc} \tag{7}$$

Hence, (1) and (3) can be transformed as (8),(9)

$$v_{dc\eta max} = \sqrt{\frac{R_2}{R_1}}\frac{\omega_0 k\sqrt{L_1 L_2}}{\sqrt{R_1 R_2 + \left(\omega_0 k\right)^2 L_1 L_2} + \sqrt{R_1 R_2}}V_s \tag{8}$$

$$\hat{k} = \frac{4V_s + \sqrt{16V_s^2 - \pi R_1 i_{dc}\left(8v_{dc} + \pi^2 R_2 i_{dc}\right)}}{\pi^2 i_{dc}\omega_0\sqrt{L_1 L_2}} \tag{9}$$

IV. Modeling and Control of DC-DC converter

In this section, modeling and control method of the DC-DC converter on the secondary side using state space averaging techniques is introduced [10]. The state space model of DC-DC converter in Fig. 5 is linearized and taken apart into

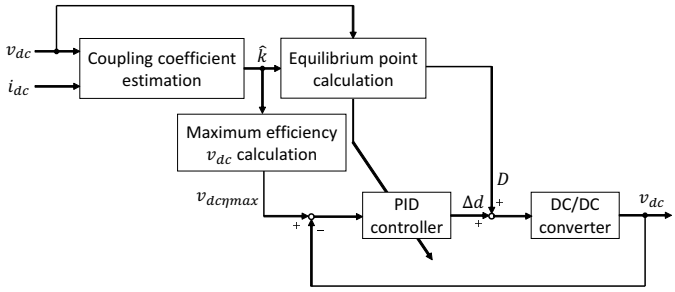

Fig. 6. Block diagram of k estimation and maximum efficiency control.

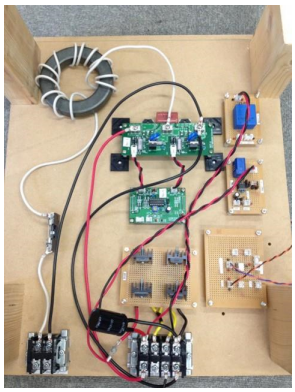

(a) DC-DC converter

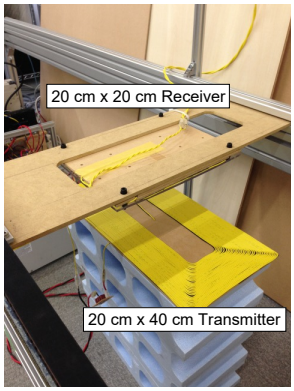

(b) Transmitter, receiver

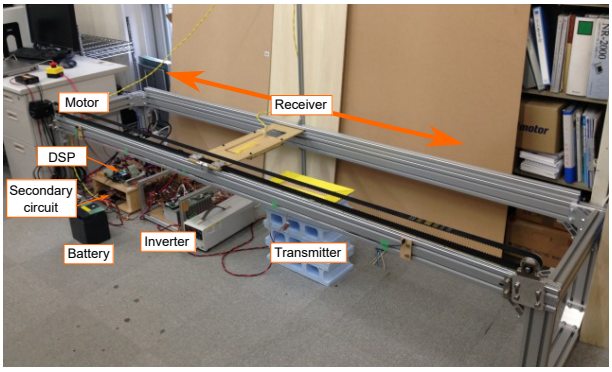

(c) Whole picture of the experimental setup

Fig. 7. Experimental setup for DWPT.

an equilibrium point and a small signal model around that equilibrium point in order to linearize its nonlinear system. In the DC-DC converter in Fig. 5, the upper switch and the lower switch are turned ON/OFF alternately so that the DC-DC converter is operated in continuous conduction mode. According to the state space model of DC-DC converter [11], the equilibrium point satisfies (10). ($d(t)$ is the duty ratio of the upper switch.)

$$V_{dc} = \frac{ED + RI_{dc}}{D^2}, \qquad I_L = \frac{I_{dc}}{D} \tag{10}$$

Where V_{dc}, I_{dc}, I_L, D are the values of $v_{dc}, i_{dc}, i_L, d(t)$ at the equilibrium point, respectively.

In this study, I_{dc} is determined by the current transfered from the primary side and calculated as (11) using (2),(7).

$$I_{dc} = \frac{8}{\pi^2} \frac{\omega_0 k \sqrt{L_1 L_2} V_s - R_1 V_{dc}}{R_1 R_2 + (\omega_0 k)^2 L_1 L_2} \tag{11}$$

From (10) and (11), D is given as (12).

$$D = \frac{E + \sqrt{E^2 - 4RV_{dc\eta max} I_{dc}|_{V_{dc}=V_{dc\eta max}}}}{2V_{dc\eta max}} \tag{12}$$

Now, the small signal model satisfies the following state space equations (13),(14).

$$\frac{d}{dt}\Delta \boldsymbol{x}(t) = \Delta \boldsymbol{A} \Delta \boldsymbol{x}(t) + \Delta \boldsymbol{B} \Delta \boldsymbol{u}(t) \tag{13}$$

$$\Delta v_{dc}(t) = \Delta \boldsymbol{c} \Delta \boldsymbol{x}(t) \tag{14}$$

$$\Delta \boldsymbol{A} = \begin{bmatrix} -\frac{R}{L} & \frac{D}{L} \\ -\frac{D}{C} & -\frac{8}{\pi^2} \frac{R_1}{C\left(R_1 R_2 + (\omega_0 k)^2 L_1 L_2\right)} \end{bmatrix}, \Delta \boldsymbol{B} = \begin{bmatrix} \frac{V_{dc}}{L} \\ -\frac{I_L}{C} \end{bmatrix}$$

$$\Delta \boldsymbol{c} = \begin{bmatrix} 0 & 1 \end{bmatrix}, \quad \Delta \boldsymbol{x}(t) = \begin{bmatrix} \Delta i_L(t) \\ \Delta v_{dc}(t) \end{bmatrix}, \quad \Delta \boldsymbol{u} = \Delta d(t)$$

From (13),(14), the transfer function from $\Delta d(s)$ to $\Delta v_{dc}(s)$ is derived as (15),

$$\frac{\Delta v_{dc}}{\Delta d} = \frac{b_1 s + b_0}{s^2 + a_1 s + a_0} \tag{15}$$

$$a_1 = \frac{R}{L} + \frac{8}{\pi^2} \frac{R_1}{C\left\{R_1 R_2 + (\omega_0 k)^2 L_1 L_2\right\}}$$

$$a_0 = \frac{1}{LC}\left\{D^2 + \frac{8}{\pi^2} \frac{RR_1}{R_1 R_2 + (\omega_0 k)^2 L_1 L_2}\right\}$$

$$b_1 = -\frac{I_L}{C}, \quad b_0 = -\frac{RI_L + DV_{dc}}{LC}$$

(15) is a second order system. Therefore, feedback control of $v_{dc}(s)$ with arbitrary poles is possible by designing the PID controller (16) through pole placement.

$$C_{PID}(s) = K_P + \frac{K_I}{s} + \frac{K_D s}{\tau s + 1} \tag{16}$$

Summarizing the above, the block diagram of real-time coupling coefficient estimation and the feedback control can be indicated in Fig. 6. From the obtained v_{dc} and i_{dc}, coupling coefficient k is estimated. Subsequently, $v_{dc\eta max}$ is calculated and used as the secondary voltage command. Meanwhile, an equilibrium point which updates the PID controller at every sampling point is calculated. Accordingly, the feedback loop is able to have the designed pole at all times.

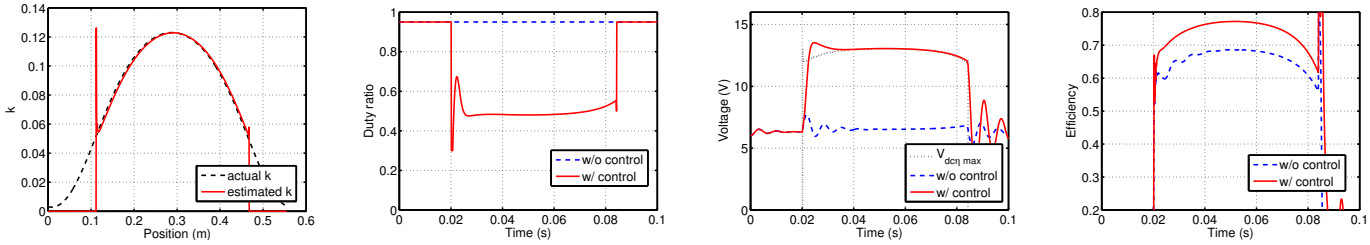

(a) k estimation (b) Duty ratio $d(t)$ (c) Secondary voltage v_{dc} (d) DC to DC efficiency η

Fig. 8. Simulation results of the proposed control.

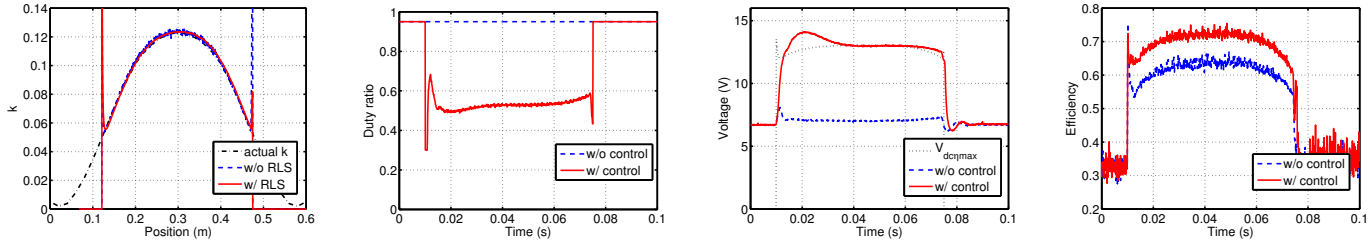

(a) k estimation (b) Duty ratio $d(t)$ (c) Secondary voltage v_{dc} (d) DC to DC efficiency η

Fig. 9. Experimental results of the proposed control.

TABLE I
PARAMETERS OF THE EXPERIMENTAL SETUP.

Parameter	Meaning	Value
f	Operating frequency	100 kHz
V_s	AC voltage source amplitude	18 V
L_1	Transmitter inductance	417.1 μH
C_1	Transmitter capacitance	6.03 nF
R_1	Transmitter resistance	1.83 Ω
L_1	Receiver inductance	208.5 μH
C_1	Receiver capacitance	12.15 nF
R_1	Receiver resistance	1.28 Ω
L	DC-DC converter inductance	1000 μH
C	DC-DC converter capacitance	1000 μF
R	DC-DC converter resistance	0.2 Ω
f_s	DC-DC converter frequency	10 kHz
E	Battery voltage	6 V

V. SIMULATION AND EXPERIMENT

In this section, the simulation and experimental results of the proposed real-time coupling-coefficient estimation and maximum efficiency control are introduced. The experimental setup is shown in Fig. 7. The whole circuit configuration used in the simulation and experiments is the same as Fig. 5. The parameters of the experimental setup are in TABLE I. In the simulation and experiments, the inverter is operated only while the receiver is above the transmitter and k is beyond 0.05 to prevent huge transmitting loss. The coupling coefficient estimation and maximum efficiency control is conducted only while the secondary circuit is receiving the power. The forgetting factor λ of RLS filter is set to 0.95. All of the four poles of the feedback loop are placed at 500 rad/sec. The sampling time of each current and voltage sensor is 20 μs. The receiving side (vehicle) drives at 20 km/h of constant speed over a transmitter. Assuming that the setup is a 1/3 scale model, the change in k is almost the same as it at 60 km/h in a real-scale DWPT system. The gap between two coils is 10 cm which has coupling coefficient k of 0.12. In the simulation, the k fluctuation of the experimental setup was simulated with an approximated polynomial.

Fig. 8 and 9 shows the simulation and experimental results of real-time coupling coefficient estimation and maximum efficiency control, respectively.

(8a) and (9a) are the simulation and experimental results of coupling coefficient estimation. The black dotted line is the actual k (measured offline). The blue line is the estimated k without RLS filter. The red line is the estimated k with RLS filter. In both simulation and experiments, estimated k matches very well with the actual k in the whole region. These results prove that the proposed k estimation method is quick and precise enough for DWPT system since there is no obvious delay in the estimation. From (9a), the RLS filter has an obvious effect on the real-time estimation because the measuring noise in the estimation is reduced.

(8b) and (9b) are the behaviors of duty ratio $d(t)$. The control of DC-DC converter was succeeded in the experiment because the both results match each other. The duty ratio $d(t)$ was reduced right after the secondary side started receiving the power to boost up the secondary voltage v_{dc}.

(8c) and (9c) are the behaviors of the secondary voltage v_{dc}. v_{dc} was boosted up and fixed around $v_{dc\eta max}$ as soon

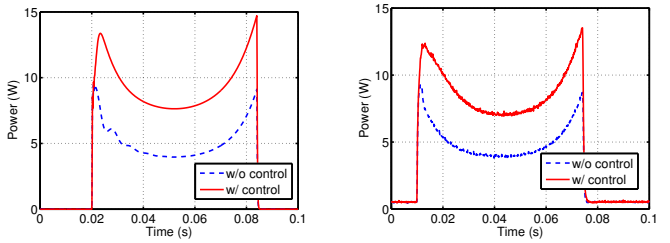

(a) Received power (simulation) (b) Received power (experiment)

Fig. 10. Simulation and experimental results of received power.

as the secondary side started receiving the power with the control although v_{dc} is fixed around the battery voltage without control. In the experimental result, the larger time delay in boosting up v_{dc} and larger damping than the simulation result can be seen. To reduce the time delay, adjustment of the DC-link capacitor and the feedback controller gain is necessary. It is important to find an optimal size of capacitance of DC-link capacitor since too large DC-link capacitor delays the response of v_{dc} and too small capacitor destabilizes v_{dc}.

(8d) and (9d) are the results of DC to DC transmitting efficiency. In the both results, the effects of the maximum efficiency control are obvious. Almost a 10 % improvement in efficiency is obtained while the receiver is moving at 20 km/h. Therefore, the proposed control method is sufficiently applicable up to 60 km/h driving in real DWPT system. The experimental result has slightly smaller efficiency than that of simulation. copper loss or converter loss which were not simulated, or small distortions of current and voltage are considered to be the main reasons for the difference.

VI. Conclusion

In this paper, the considered DWPT system was proposed. A simple primary transmitting system is needed to make installation and maintenance easy. On the other hand, a secondary receiving system should control transmitting efficiency or received power precisely.

The ideas of real-time coupling coefficient estimation and maximum efficiency control using simplified models were proposed. Moreover, the modeling and control method of DC-DC converter on the secondary side with PID feedback controller were explained. The whole estimation and control method are not too complicated and easily summarized in Fig. 6. Lastly, the simulation based on the experimental setup and the actual experiment were carried out. The simulation and experimental results matched each other and these showed that the proposed control can sufficiently improve the transmitting efficiency even while EVs are in motion. This study still have many possibilities to be improved by optimizing the DC-link capacitor, PID controller and so on.

The analysis on responsiveness of the proposed control is considered as a good future work. Furthermore, whole transmitting efficiency including converter losses at an inverter, a rectifier, a DC-DC converter is also going to be considered.

References

[1] A. Kurs, A. Karalis, R. Moffatt, J. D. Joannopoulos, P. Fisher, and M. Soljacic, "Wireless power transfer via strongly coupled magnetic resonances," *Science*, Vol. 317, no. 5834, pp.83-86, 2007.

[2] Z. Wang, Y. Li, Y. Sun, C. Tang, X. Lv, "Load Detection Model of Voltage-Fed Inductive Power Transfer System", *IEEE Transactions on Power Electronics*, Vol. 28, No. 11, 2013.

[3] K. Futopoulou, B. Flynn, "Wireless Power Transfer in Loosely Coupled Links: Coil Misalignment Model," *IEEE Transactions on Magnetics*, Vol. 47, No. 2, 2011.

[4] S. Li, C. C. Mi, "Wireless Power Transfer for Electric Vehicle Applications," *Emerging and Selected Topics in Power Electronics*, Vol. 3, pp.4-17, 2015.

[5] J. Shin, S. Shin, Y. Kim, S. Ahn, S. Lee, G. Jung, S. J. Jeon, D. H. Cho, "Design and Implementation of Shaped Magnetic -Resonance-Based Wireless Power Transfer System for Roadway-Powered Moving Electric Vehicles," *IEEE Transactions on Industrial Electronics*, Vol. 61, no.3, pp.1179-1192, 2014.

[6] S. Raabe, G. A. Covic, "Practical Design Considerations for Contactless Power Transfer Quadrature Pick-Ups," *IEEE Transactions on Industrial Electronics*, Vol. 60, no.1, pp.400-409, 2013.

[7] W. Li, C. C. Mi, S. Li, "Integrated LCC Compensation Topology for Wireless Charger in Electric and Plug-in Electric Vehicles," *IEEE Transactions on Industrial Electronics*, Vol. 62, pp.4215-4225, 2015.

[8] H. Hao, G. A. Covic, J. T. Boys, "An Approximate Dynamic Model of LCL-T-Based Inductive Power Transfer Power Supplies," *IEEE transactions on Power Electronics*, Vol. 29, no. 10, 2014.

[9] M. Kato, T. Imura, Y. Hori, "Study on Maximize Efficiency by Secondary Side Control Using DC-DC Converter in Wireless Power Transfer via Magnetic Resonant Coupling," *IEEE, EVS27*, pp.1-5, 2013.

[10] K. Hata, T. Imura, Y. Hori, "Maximum Efficiency Control of Wireless Power Transfer via Magnetic Resonant Coupling Considering Dynamics of DC 窶泥 C Converter for Moving Electric Vehicles," *The Applied Power Electronics Conference and Exposition*, pp. 3301-3306, 2015.

[11] D. Kobayashi, T. Imura, Y. Hori, "Real-time coupling coefficient estimation and maximum efficiency control on dynamic wireless power transfer for electric vehicles," *Emerging Technologies: Wireless Power (WoW), 2015 IEEE PELS Workshop on*, pp. 1-6, 2015.

[12] L. Chen, G. R. Nagendra, J. T. Boys, G. A. Covic, "Double-Coupled Systems for IPT Roadway Applications," *Emerging and Selected Topics in Power Electronics*, Vol. 3, pp.37-49, 2015.

[13] S. Choi, J. Huh, W. Y. Lee, S. W. Lee, C. T. Rim, 窶迪 ew Cross - Segmented Power Supply Rails for Roadway-Powered Electric Vehicles," *IEEE transactions on Power Electronics*, Vol. 28, No.12, pp.5832-5841, 2013.

[14] K. Lee, Z. Pantic, S. M. Lukic, "Reflexive Field Containment in Dynamic Inductive Power Transfer Systems," *IEEE Transactions on Power Electronics*, Vol. 29, no.9, pp.4592-4602, 2014.

[15] J. Vissuta, T. Imura, Y. Hori, "Coupling Coefficients Estimation of Wireless Power Transfer System via Magnetic Resonance Coupling using Information from Either Side of the System," *IB2COM 2012*, 2012.

[16] K. Hata, T. Imura, Y. Hori, "Dynamic Wireless Power Transfer System for Electric Vehicle to Simplify Ground Facilities - Power Control Based on Vehicle-side Information -," *EVS28*, 2015.